

# Orthogonal analysis of functional gold nanoparticles for biomedical applications

De-Hao Tsai<sup>1,2</sup> · Yi-Fu Lu<sup>2</sup> · Frank W. DelRio<sup>1</sup> · Tae Joon Cho<sup>1</sup> · Suvajyoti Guha<sup>3</sup> · Michael R. Zachariah<sup>3,4</sup> · Fan Zhang<sup>1</sup> · Andrew Allen<sup>1</sup> · Vincent A. Hackley<sup>1</sup>

Received: 22 July 2015 / Revised: 17 August 2015 / Accepted: 26 August 2015 / Published online: 11 September 2015  
© Springer-Verlag Berlin Heidelberg 2015

**Abstract** We report a comprehensive strategy based on implementation of orthogonal measurement techniques to provide critical and verifiable material characteristics for functionalized gold nanoparticles (AuNPs) used in biomedical applications. Samples were analyzed before and after  $\approx 50$  months of cold storage ( $\approx 4$  °C). Biomedical applications require long-term storage at cold temperatures, which could have an impact on AuNP therapeutics. Thiolated polyethylene glycol (SH-PEG)-conjugated AuNPs with different terminal groups (methyl-, carboxylic-, and amine-) were chosen as a model system due to their high relevancy in biomedical applications. Electrospray-differential mobility analysis, asymmetric-flow field flow fractionation, transmission electron microscopy, scanning electron microscopy, atomic force microscopy, inductively coupled plasma mass spectrometry, and small-angle X-ray scattering were employed to provide both complementary and orthogonal information on (1) particle size and size

distribution, (2) particle concentrations, (3) molecular conjugation properties (i.e., conformation and surface packing density), and (4) colloidal stability. Results show that SH-PEGs were conjugated on the surface of AuNPs to form a brush-like polymer corona. The surface packing density of SH-PEG was  $\approx 0.42$  nm<sup>-2</sup> for the methyl-PEG-SH AuNPs,  $\approx 0.26$  nm<sup>-2</sup> for the amine-SH-PEG AuNPs, and  $\approx 0.18$  nm<sup>-2</sup> for the carboxylic-PEG-SH AuNPs before cold storage, approximately 10 % of its theoretical maximum value. The conformation of surface-bound SH-PEGs was then estimated to be in an intermediate state between brush-like and random-coiled, based on the measured thicknesses in liquid and in dry states. By analyzing the change in particle size distribution and number concentration in suspension following cold storage, the long term colloidal stability of AuNPs was shown to be significantly improved via functionalization with SH-PEG, especially in the case of methyl-PEG-SH and carboxylic-PEG-SH (i.e., we estimate that >80 % of SH-PEG5K remained on the surface of AuNPs during storage). The work described here provides a generic strategy to track and analyze the material properties of functional AuNPs intended for biomedical applications, and highlights the importance of a multi-technique analysis. The effects of long term storage on the physical state of the particles, and on the stability of the ligand-AuNP conjugates, are employed to demonstrate the capacity of this approach to address critical issues relevant to clinical applications.

**Electronic supplementary material** The online version of this article (doi:10.1007/s00216-015-9011-9) contains supplementary material, which is available to authorized users.

✉ De-Hao Tsai  
dhtsai@mx.nthu.edu.tw

✉ Vincent A. Hackley  
vince.hackley@nist.gov

<sup>1</sup> Materials Measurement Science Division, National Institute of Standards and Technology, Gaithersburg, MD 20899, USA

<sup>2</sup> Department of Chemical Engineering, National Tsing Hua University, Hsinchu, Taiwan, Republic of China

<sup>3</sup> Chemical Sciences Division, National Institute of Standards and Technology, Gaithersburg, MD 20899, USA

<sup>4</sup> Departments of Chemical Engineering and Chemistry, University of Maryland, College Park, MD 20740, USA

**Keywords** Nanoparticles · Nanotechnology, Interface · Surface analysis, Kinetics

## Introduction

Gold nanoparticles (AuNPs), principally in colloidal form, are one of the most promising building blocks for biomedically-

relevant nanoparticle enabled products (NEPs) and applications [1–6]. AuNPs have the advantageous property of tunable surface plasmon resonance (SPR) [7], an optical phenomenon that has been exploited for applications ranging from imaging and optical-based molecular detection to hyperthermal therapy for cancer treatment, combined with facile synthetic methods [8] and general biocompatibility [9]. Furthermore, thiol-Au chemistry provides an effective route for rational design by surface modification (i.e., attachment of functional molecules to the surface of AuNPs). By conjugation with drug ligands, for example, AuNPs can function as stealthy vectors to improve drug-delivery efficacy [6, 10–12]. The concept of applying AuNPs in nanomedicine is attractive, because in theory they can provide a therapeutic synergetic effect while avoiding or mitigating harm to healthy tissue [1, 6, 10].

In order to achieve the desired functionality described above, it is necessary to identify and make use of AuNPs with suitable material properties. For this, the concept of materials-by-design offers a powerful and fascinating platform. A major challenge for successful implementation of the design is the accurate and precise specification of material properties for AuNPs in NEPs (defined as AuNP-NEPs), including batch-to-batch uniformity. On this basis, it is of essential importance to understand the correlations between the properties of the materials in design and their formulation chemistry. However, serious questions have been raised about the quality of NEPs, where the uncertainties in the accuracy of material property measurements lead to challenges in assessing and understanding the results of their corresponding efficacy and safety. Specifically, validated measurement methods do not exist to sufficiently assess the purity of NEPs or to compare nanomaterials from different vendors or laboratories. These general, yet crucial concerns, if unaddressed, could adversely affect the eventual implementation of these promising AuNP-NEPs. For example, to preclude potential hazards to human health, regulators may halt or disapprove the use of these AuNP-NEPs for biomedical applications.

From the perspective of product development and quality assurance, it is critical to have suitable AuNPs characterized by traceable characterization methods. The development of standard reference materials has partially satisfied the need for traceability in AuNP size measurements. Similarly, to obtain complete information of material properties for AuNP-NEPs, it is necessary to establish suitable measurement metrology and methodology, the importance of which has been recognized by regulatory agencies and pharmaceutical companies world-wide [1, 13, 14]. Once established, material characterization will help bridge the gap between AuNP-NEP design and performance, and facilitate the screening of AuNP-NEPs for disqualifying properties prior to performing laborious and expensive biological tests [13, 14].

Physical dimensions (including surface area), surface properties, colloidal stability, and particle concentration are

considered among the most important material properties for applications in nanomedicine. Among these properties, physical dimensions, especially the primary and/or secondary particle diameter, have arguably the greatest impact on the AuNP functionality (e.g., transport behavior, circulation half-life, ligand loading, drug dosage, etc.). For example, to avoid renal filtration through the glomerular capillary wall in the kidney, while still being able to target and accumulate at a tumor site without recognition by the reticuloendothelial system (RES), the acceptable primary diameter for sphere-like AuNPs should range from about 10 to 100 nm [15, 16]. Therefore, physical dimensions are always the first consideration during the design and formulation of a NEP.

Similarly, surface properties of AuNPs determine their interactions with ligands, cells, or physiological systems in the human body (e.g., hemolytic properties), affecting the therapeutic performance and biodistribution of AuNP-NEPs [17]. Surface engineering of AuNPs with targeting moieties via thiol-Au chemistry has proven advantageous, where transport properties (including circulation time), imaging/diagnostic ability, and drug loadings can be enhanced by judiciously choosing suitable ligands [18]. In the design phase, knowledge of the type of ligand that binds to the surface of AuNPs, ligand surface-packing density, and its molecular conformation at the surface is the key to modify and optimize AuNP-NEP performance. Surface packing density is determined by a combination of the binding affinity of ligands with the AuNP surface, the equilibrium ligand/AuNP concentration used in the formulation, and the size/structure of the ligand (e.g., steric effects can reduce packing density). Molecular conformation is determined by the interactions between the surface-bound ligands and the biological medium, including the number of ligands existing on the Au surface. In general, AuNPs grafted with a high-packing-density, neutral polymer corona (e.g., thiolated polyethylene glycol, SH-PEG) on the surface are more transportable and less likely to be recognized by the RES, resulting in an increased efficacy in the delivery of drug ligands [1, 10, 11, 19, 20]. In addition to the transport properties, a variety of desirable functionalities can be transferred to AuNPs by modifying the Au surface through ligand conjugation. For example, the drug cisplatin has been studied for its application in chemo-radiation therapy [6]. Through design and engineering of the AuNP surface with ligands that have both thiol and carboxylic end groups, cisplatin can be complexed to the AuNP-based platform, delivered to the tumor cells, and released on target or enhanced by the synergetic stimulated emission of photoelectrons and Auger electrons from both the Au and Pt components. With the concept of surface modification, the effective dosing and targeting can be improved relative to the therapeutic application of traditional small molecule drugs.

Colloidal stability of AuNPs is an important factor for the production and application AuNP-NEPs. Agglomeration/

aggregation is the principal result of poor or uncontrolled colloidal instability, occurring due to the strong van der Waals attractive force between AuNPs. The physical dimensions (mainly secondary size) generally change over time once agglomeration/aggregation begins [6, 13, 14, 21]. This non-equilibrium process directly leads to decline of both the transport properties and imaging/diagnostic capacity (e.g., via quenching of the SPR effect), which cause difficulties in the construction of correlations between the designed material properties and the therapeutic performance. Because of the issues described above, colloidal stability has to be considered at the outset in the design and formulation of AuNP-NEPs, not just in the native suspension but under use conditions and in biological fluids.

Another important factor is the concentration of particles needed to deliver a required dose in therapeutics, or to exhibit the required sensitivity for imaging and diagnostic applications [6, 21]. As discussed previously, the surface area of AuNPs is a key factor for dosing, as it sets limits for the maximum number of ligands that can be carried by a single particle. An increase in the concentration of primary particles is expected to increase the total surface area in NEPs and concomitantly the therapeutic load. To monitor both dose and biodistribution, it is necessary to have particle concentration above the detection limit for the measurement of choice [13, 14]. In general, these properties are correlated or interrelated, making it a challenge to differentiate dependencies and develop clear structure–property–performance criteria. For example, particle size and number concentration of AuNPs can be strongly affected by colloidal stability over time; on the other hand, surface properties significantly impact the colloidal stability and the resulting physical state [6, 11, 21].

In this work, we propose an orthogonal multi-technique characterization approach as a viable strategy to interrogate correlations between key material properties and the efficacy and safety of AuNP-NEPs. We focus on investigations of particle size and size distribution, number-based and mass-based concentration, surface properties (e.g., packing density, binding affinity, and conformation), and colloidal stability. As a test bed, we employ SH-PEG-conjugated AuNPs with different terminal groups, due to the relevance of PEG in biomedical applications [1, 10, 11, 19, 20]. We also examine the changes that occur during extended cold storage ( $\approx 4$  °C) over a period of  $\approx 50$  months, shedding light on the chemical stability of the ligand–Au complex and its relationship to colloidal stability of the functionalized particles. For nanomedicine platforms, long term storage, particularly at reduced temperatures, could potentially alter the physical and chemical state, thus impacting their therapeutic efficacy. Studies of long term cold storage of functionalized nanomaterials in aqueous-based suspensions are virtually non-existent in the peer reviewed literature. To our knowledge, this is also the longest cold storage study of functionalized AuNPs reported in the literature.

Our objectives are (1) to develop a methodology to perform pre-screening prior to AuNP-NEP use in biomedical applications and clinical evaluations, and (2) to identify and quantify key properties of these materials that may provide scientific insight into the correlations between material properties and therapeutic performance (e.g., the size effect).

## Experimental methods

### Materials

Four types of surface-modified AuNP colloids were obtained from Nanopartz [22] (Loveland, CO, USA): citrate-stabilized (“unconjugated”), methyl-terminated-SH-PEG (m-SH-PEG-AuNPs), carboxyl-terminated-SH-PEG (c-SH-PEG-AuNP), and amine-terminated-SH-PEG (a-SH-PEG-AuNP). The diameter of the AuNP core is  $\approx 20$  nm for all samples. The starting concentration (at  $t=0$ ) is unknown for all samples. The molar mass of the SH-PEG,  $M_m$ , is 5 kDa (i.e., SH-PEG5K, based on the vendor’s information). Aqueous ammonium acetate (Sigma-Aldrich, >98 %, USA) solution was used to adjust the ionic strength of samples and to perform electrospray ionization. All chemicals were used as received without further purification. Biological grade 18.2 M $\Omega$ ·cm deionized water (Millipore, Billerica, MA, USA; Aqua Solutions, Jasper, GA, USA) was used to prepare solutions and colloidal suspensions. The pH of the unconjugated AuNP, m-SH-PEG-AuNP, c-SH-PEG-AuNP, and a-SH-PEG-AuNP suspensions, was measured as 7.8, 7.0, 7.3 and 3.9, respectively. These materials were analyzed and compared before and after long term cold storage ( $\approx 50$  months) at 4 °C;  $t=0$  months refers to as-received material prior to cold storage.

### Electrospray-differential mobility analysis

The electrospray-differential mobility analysis (ES-DMA) was used to obtain a number-based particle size distribution [11, 23, 24]. Briefly, the electrospray (ES) aerosol generator (model 3480, TSI Inc., Shoreview, MN, USA) was used to aerosolize AuNPs. Then the aerosolized AuNPs were delivered to an electrostatic classifier (model 3081, TSI Inc.), where the particles were classified based on their electric mobility under an applied DC electric field. Particles of a specific mobility size,  $d_{p,m}$ , that exited the electrostatic classifier were counted by a condensation particle counter (CPC, model 3775 or model 3025, TSI Inc.). The step size used in the particle size measurements was 0.2 nm and the time interval between each step size was 10 s. Sample flow rate ( $Q_{\text{samp}}$ ) in the DMA was set to 1.2 L min $^{-1}$  and sheath flow rate ( $Q_{\text{sh}}$ ) in the DMA was 10.0 L min $^{-1}$  or 30 L min $^{-1}$ . The uncertainty in the measurement of  $d_{p,m}$  was estimated to be 0.3 nm in this study, using one standard deviation of triplicate measurements.

## Asymmetric-flow field flow fractionation

The asymmetric-flow field flow fractionation (A4F) system consists of a high-performance isocratic pump (1100 series, Agilent Technologies, Santa Clara, CA, USA), manual injection valve (Rheodyne 7725i, IDEX Corporation, Oak Harbor, WA, USA) with a 100  $\mu\text{L}$  stainless steel sample loop, field/flow control module and A4F separation channel (Eclipse 2, Wyatt Technology, Santa Clara, CA, USA), multi-angle light scattering (MALS) detector (Dawn Heleos, Wyatt Technology) and ultraviolet–visible (UV–Vis) diode array detector (1200 DAD, Agilent Technologies). Regenerated cellulose membrane (molar mass cut-off=10 kDa, Wyatt Technology) was used for all A4F experiments. A 350  $\mu\text{m}$  spacer was used to define the depth of the A4F channel for all separation experiments reported here. The mobile phase for A4F separation was 0.02 % aqueous sodium azide solution. The cross flow rate was 2  $\text{mL min}^{-1}$  and the channel flow was 0.5  $\text{mL min}^{-1}$ . [Details of the A4F method, including the estimation of particle size based on retention time, have been described in our previous publications and are summarized in the [Electronic Supplementary Material \(ESM\)](#) [23]. At least two replicate fractograms were measured by A4F for each condition.

## Electron and atomic force microscopy

The primary structures of AuNP samples were imaged using a transmission electron microscope (TEM, JEM-2100HT, JEOL, Tokyo, Japan) at an acceleration voltage of 80 kV. The drop-cast method was used to prepare samples for TEM analysis. To image and understand the extent of particle aggregation, we use a scanning electron microscope (SEM, Hitachi SU8010, Hitachi, Japan) operated at 10 kV and an atomic force microscope (AFM, Dimension 3100, Veeco, Santa Barbara, CA, USA) operated in intermittent-contact (tapping) mode. Positively-charged aerosolized AuNPs were delivered to an electrostatic precipitator and deposited onto a silicon chip operated at a sample flow rate of  $\approx 1.5 \text{ L min}^{-1}$  and an electric field of  $-(2 \text{ to } 5) \text{ kV cm}^{-1}$  [23]. Due to electrostatic repulsion, deposition-induced aggregation is negligible under these conditions.

## Inductively coupled plasma mass spectrometry

An inductively coupled plasma mass spectrometer (ICP-MS, Model 7500x, Agilent Technologies) was used to measure the mass fraction of Au in solution. Samples were diluted by a factor of 10,000 using 10 % aqua regia (volume basis) prior to measurements. Uncertainty was evaluated as one standard deviation of at least two replicate measurements.

## Ultra-small angle X-ray scattering

Ultra-small angle X-ray scattering (USAXS) measurements are a modified form of small-angle X-ray scattering (SAXS) that extends the technique to smaller scattering angles and larger scattering features. Other than correction for the slit-smear geometry, data reduction and analysis proceeds in a similar way to that for conventional SAXS measurements. USAXS experiments were performed at sector 15ID-D at the Advanced Photon Source, Argonne National Laboratory using a Bonze-Hart instrument with slit-smear geometry [25]. The X-ray energy was 10 keV, which corresponds to a wavelength of 0.124 nm. Standard liquid cells with Kapton windows were used as sample containers, in which the effective sample thickness was 1 mm. The incident photon flux on the sample was  $\approx 10^{13} \text{ photon s}^{-1}$ . We acquired scattering data in a  $q$  range between  $1.5 \times 10^{-3} \text{ nm}^{-1}$  and  $10 \text{ nm}^{-1}$ . Here,  $q = 4\pi/\lambda \times \sin(\theta)$ , where  $\lambda$  is the X-ray wavelength and  $2\theta$  is the scattering angle. Average acquisition time for each data point was 1 s, and there were 200 points in each scan.

## Results and discussion

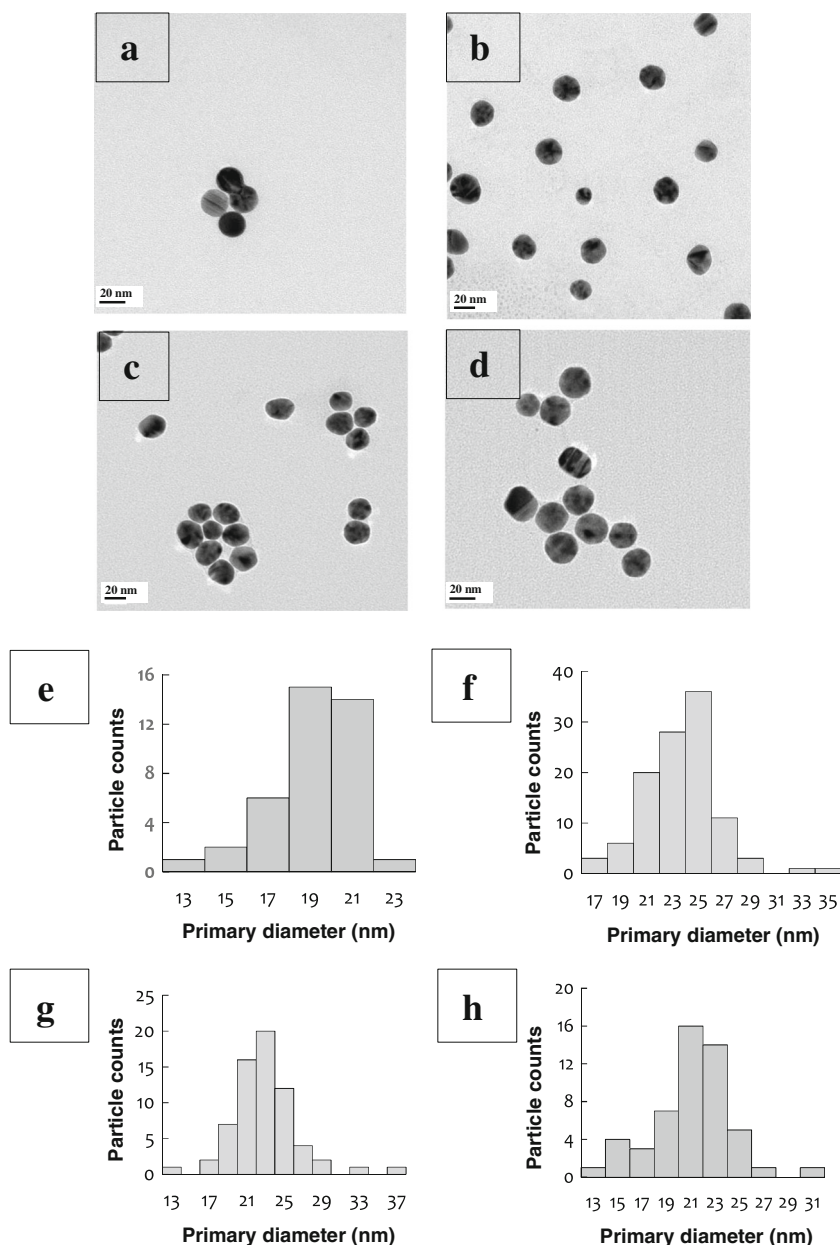
### Particle size and size distribution

As discussed previously, dimensional properties, including the primary and secondary particle diameter, particle shape, and the width of particle size distribution are very important to AuNP-based therapeutics. These dimensional properties are shown to be strong indicators for the amount of drug loading and transport to the diseased cells for applications in targeted drug delivery (e.g., enhanced permeation and retention effect, active targeting, blood circulation time). We have utilized different characterization techniques to provide comprehensive information on the dimensional properties of AuNPs.

TEM was first employed to evaluate the diameter of primary (core) particles. Figure 1a–d show representative images (additional TEM images are included in the [ESM](#)) of unconjugated AuNPs, m-SH-PEG-AuNPs, c-SH-PEG-AuNPs, and a-SH-PEG-AuNPs, respectively. The AuNPs are predominantly spheroidal (with facets apparent) and have a primary particle peak diameter centered at  $\approx (20 \text{ to } 24) \text{ nm}$  with  $\approx (5 \text{ to } 6) \text{ nm}$  full width at half maximum (see Fig. 1e–h). We note that the surface corona of SH-PEG5K is not visible due to its low electron contrast, and, as such, the presence of the SH-PEG5K corona has no significant impact on measurement of the core size. The samples were imaged after a storage period of  $\approx 50$  months at  $4^\circ\text{C}$ . Since Au has a very high chemical stability, we assume that the primary structure was largely retained.

We analyzed the USAXS data for (SH-PEG)-conjugated AuNPs, before cold storage, within the framework of *Irena*,

**Fig. 1** Morphology and primary diameter of AuNPs obtained by TEM after cold storage for  $\approx 50$  months. Representative TEM images of **a** unconjugated AuNPs, **b** m-SH-PEG-AuNPs, **c** c-SH-PEG-AuNPs, and **d** a-SH-PEG-AuNPs. Histograms of primary size for **e** unconjugated AuNPs ( $N=39$ ;  $N$  is the number of particle measured), **f** m-SH-PEG-AuNPs ( $N=109$ ), **g** c-SH-PEG-AuNPs ( $N=66$ ), and **h** a-SH-PEG-AuNPs ( $N=51$ ). Following cold storage, samples were prepared by the drop-cast method



an *Igor Pro*-based small-angle scattering analysis suite [26]. In our analysis, we assume the AuNPs are simple spheres with uniform scattering length density, and that their diameters follow a Gaussian-type volume-size distribution. Details of the USAXS analysis can be found in the *ESM*. The fitted diameters and the Gaussian full width at half maximum of the primary particle size distributions are summarized in Table 1. We found that the core diameter of (SH-PEG)-conjugated AuNPs identified by TEM (Fig. 1) and USAXS are consistent, as expected. The primary core diameter from USAXS is statistically identical for the three samples, confirming that primary core size does not change during cold storage. While TEM is visual and direct, USAXS has the advantage of being statistically significant as it probes a much larger sample population.

Corresponding USAXS derived volume size distributions for the primary particles are provided in Section 4.1 of the *ESM*.

An interesting aspect of the USAXS results is that both m-SH-PEG-AuNP and c-SH-PEG-AuNP scattering profiles are well accounted for by a single population of primary particles

**Table 1** Primary size parameters of (SH-PEG)-conjugated AuNPs from USAXS analysis of samples prior to cold storage

	Diameter (nm)	Gaussian width (nm)
m-SH-PEG-AuNPs	21.4	2.4
c-SH-PEG-AuNPs	21.6	2.3
a-SH-PEG-AuNPs	21.6	2.2

(see *ESM* section 4). This serves as strong testimony to the stability of these species, i.e., no particle aggregation is detected. The USAXS data for a-SH-PEG-AuNPs, on the other hand, cannot be described by primary particles alone. A small secondary population with a nominal diameter at  $\approx 101$  nm and a broad size distribution has to be included to ensure a quality fit. The presence of this small secondary population suggests some aggregation of AuNPs in this particular sample (i.e., least stable among the three (SH-PEG)-conjugated AuNPs). Further implications of this finding are discussed later.

ES-DMA was employed to characterize the full particle size distributions, where we can obtain the primary diameter of AuNPs and the secondary structure size. Figure 2a shows the particle size distributions for AuNPs measured by ES-DMA prior to cold storage. For the unconjugated sample, we observed AuNPs with different aggregation states (i.e., monomers, dimers, and trimers). The presence of aggregates in the as-received material is attributed to the synthesis process and relatively high solids content [21, 23], and is beyond the scope of this study. For the three SH-PEG-AuNP samples, we observed only peaks representing the monomer (primary) AuNPs, indicating that aggregates were absent from these as-received samples (i.e., below the detection limit for ES-

DMA). The observation is consistent with our findings from AFM (Fig. 2b, showing only m-SH-PEG-AuNP as an example). We attribute this lack of aggregation to the steric repulsion between the surface-bound SH-PEG coronas that reduces the binding affinity between the particles. For the unconjugated AuNP sample, the peak diameter of monomers ( $n=1$ ) was 23.3 nm, slightly higher than the values measured by TEM (Fig. 1), USAXS (Table 1), and AFM ( $\approx 21$  nm, Figs. 2b and 3). The difference may be due to the measurement physics in determination of the diameter of these spheroidal AuNPs as shown in a previous study [27]. For example, ES-DMA measures the particle's diameter based on its electrical mobility, which may be different than its two-dimensional projected length as measured by TEM, its three-dimensional electron density arrangement as measured by USAXS, and its height as measured by AFM. We also observed the peak diameter of the SH-PEG-AuNPs was  $\approx (5$  to  $7)$  nm larger than that of the unconjugated AuNP monomers, but we will defer the discussion on this point to the next section.

Orthogonally, we use A4F, a solution-phase chromatographic-like approach, to obtain fractograms of the dispersed particles with retention time converted to equivalent spherical hydrodynamic diameter using a calibration described in the

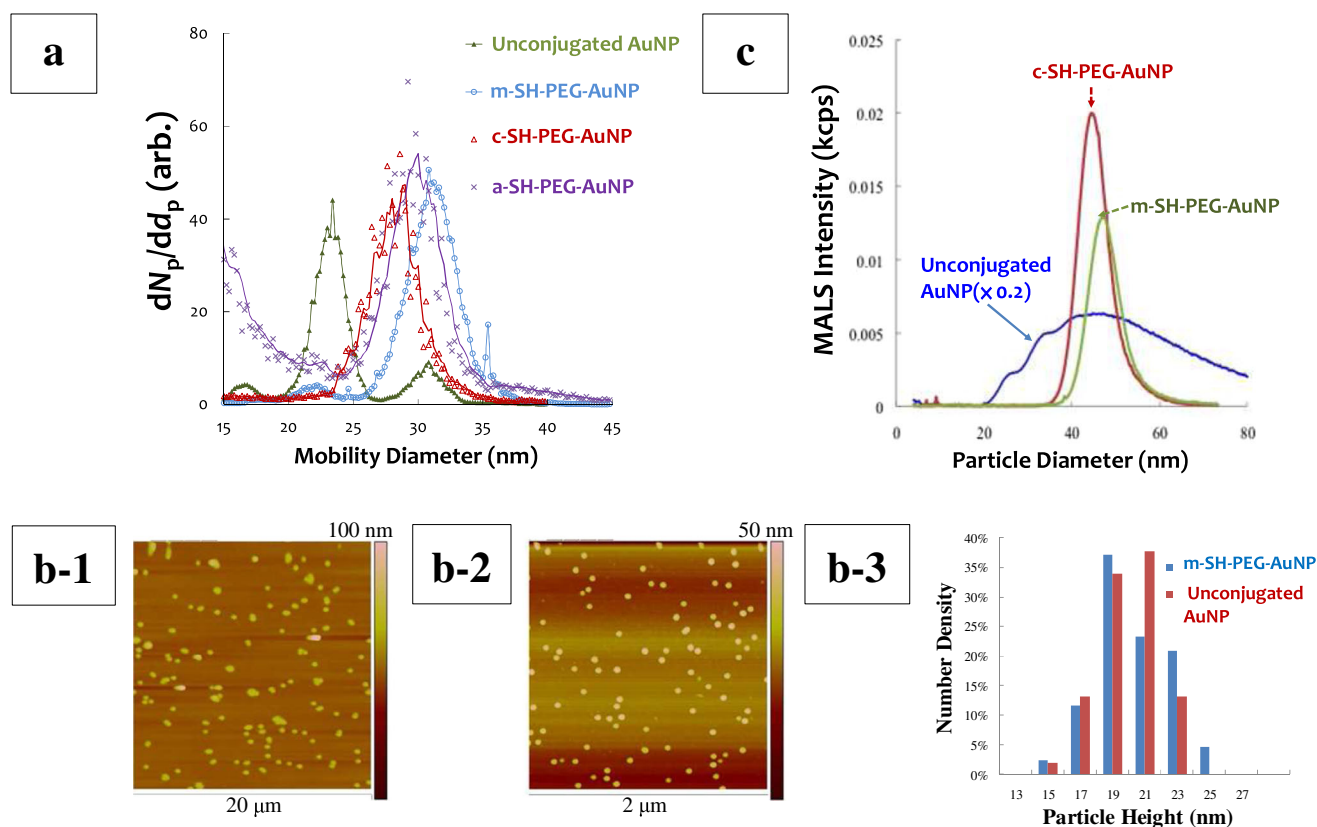


**Fig. 2** Characterization of particle size prior to cold storage ( $t=0$  months) for AuNP samples using orthogonal techniques. **a** Particle diameter distributions measured by ES-DMA.  $Q_{sh}=30$  L  $\text{min}^{-1}$ . Here  $N_p$  is the number concentration of aerosolized AuNPs and  $d_p = d_{p,m}$ . **b** AFM

measurements: **b-1**: representative image of unconjugated AuNPs, **b-2**: representative image of m-SH-PEG-AuNPs. **b-3**: histogram of unconjugated AuNP and m-SH-PEG-AuNP samples. **c** A4F fractograms

ESM [23]. As shown in Fig. 2c, we observed a multi-modal, intensity-based particle size distribution for the unconjugated AuNP sample, confirming the presence of discrete size AuNP clusters measured by ES-DMA and AFM. A4F identified the peak size of the monomers at  $\approx 24$  nm, which is close to the results found by TEM and ES-DMA ( $n=1$ ). A possible reason of cluster formation can be attributed to the relatively high concentration of the present samples ( $>2000$  ppm) in comparison to other AuNP samples (including NIST RM 8011, 8012 and 8013) used in the previous studies [28]. For m-SH-PEG-AuNPs and c-SH-PEG-AuNPs, the peaks corresponding to discrete populations of AuNP clusters are absent, consistent with results obtained by ES-DMA, AFM and USAXS. Moreover, for the SH-PEG5K-conjugated AuNPs, the peak diameters measured by ES-DMA and A4F differ. This difference will be addressed in the next section. Combining the data shown in Figs. 1 and 2, we obtain a complete set of information on primary particle size, secondary particle size, particle morphology, and particle size distribution. Note that we were unable to measure a-SH-PEG-AuNPs using the A4F due to the strong interaction with the negatively charged membrane surface (i.e., low recovery and poor separation).

### Surface properties

Using a core-shell analogy, the difference in particle size between the unconjugated and SH-PEG-AuNPs, as measured by ES-DMA and A4F prior to cold storage, can be correlated to the PEG corona thickness on the AuNP core. Assuming the conformation of SH-PEG in the dry state is independent of the environmental condition in solution, the increase in  $d_{p,m}$  with SH-PEG conjugation calculated from the data at  $t=0$  months in Fig. 2a can be used to obtain the initial surface packing density of SH-PEG5K on the AuNPs. Using a previously-developed analytical model [16], the surface packing density of the SH-PEG5K,  $\sigma$ , was calculated based on the increased mobility diameter,  $\Delta d_{p,m}$ , measured by ES-DMA as given by,

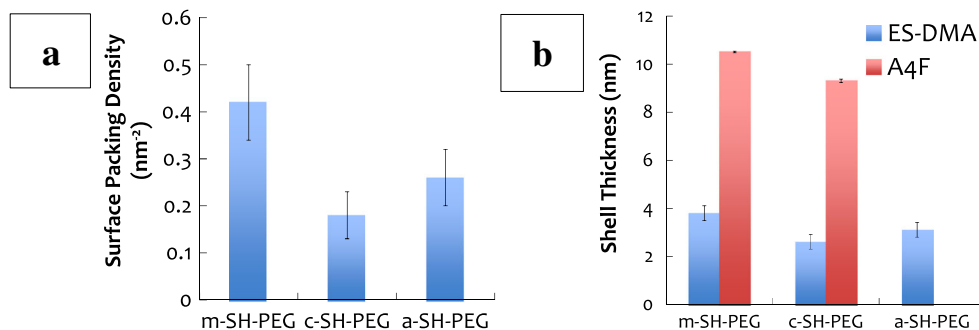
$$\sigma = \frac{[(d_{p,m} + \Delta d_{p,m})^2 - d_{p,m}^2]^2}{[2d_{p,m} < x^2 >]^2} \tag{1}$$

where  $<x^2>^{1/2}$  is the random-walk radius of SH-PEG5K, given

by  $<x^2>^{1/2} = cN_b^a N_k^a l_b$  where  $l_b$  is the length of the monomer segment ( $l_b=0.44$  nm),  $c$  is the interaction constant between polymer and particle surface ( $c=0.62$  for end-anchored polymers),  $N_k$  is the number of statistical bases per segment ( $N_k=1.6$ ),  $N_b$  is the number of segments per polymer ( $N_b \approx 113$  for  $M_m \approx 5$  kDa), and  $a$  is constant adjusted by the polymer's interaction with the solvent [29]. In a dry condition (i.e., measured by DMA) we assume  $a=0.5$  since no extra interactions like electrostatic and hydrophobic interactions with the solvent [29]. Using Eq. (1), the surface packing density was found to be  $0.42 \text{ nm}^{-2}$ ,  $0.18 \text{ nm}^{-2}$ , and  $0.26 \text{ nm}^{-2}$ , for m-SH-PEG-AuNP, c-SH-PEG-AuNP, and a-SH-PEG-AuNP, respectively (Fig. 3a). Results suggest that the presence of carboxyl or amine sites may reduce packing density as a result of electrostatic repulsion between the surface-bound SH-PEG5K.

USAXS probes the spatial inhomogeneities in the scattering length density over the nanometer- to micrometer-scale. For SH-PEG-AuNPs, the surface corona has a different scattering length density when compared with both the solvent and the Au core. Therefore, in principle, when data quality allows, information related to the surface corona could be extracted from a proper USAXS analysis. Based on this presumption, we applied a simple core-shell model to probe the molecular configuration of the polymeric corona on the AuNP surface in the solution phase prior to cold storage. In this model, we assumed both the core and the shell possess uniform scattering length density  $\rho_c$  and  $\rho_s$ , respectively. Given the non-optimal quality of the USAXS data, we only explore this feasibility using the USAXS data for m-SH-PEG-AuNPs, and its detailed analysis can be found in the ESM. In this analysis, a nominal diameter for the AuNPs was determined at 21.3 nm, a shell thickness at 1.7 nm, and scattering length density difference between the shell and the solvent of  $0.22 \times 10^{10} \text{ cm}^{-2}$ . Based on a calculated scattering length for PEG5K of  $4.73 \times 10^{-14} \text{ m}$ , we found that the scattering intensity can be accounted for with  $\approx 1295$  PEG5K molecules per particle, which translates to a surface packing density of  $0.91 \text{ nm}^{-2}$  for m-SH-PEG-AuNP. This value is twice that obtained from ES-DMA analysis, but both values are of the same order of magnitude, which suggests that there might be validity to this core-shell analysis. However, we stress that the USAXS data

**Fig. 3** Analysis of SH-PEG5K corona on AuNP surface at  $t=0$  months (prior to cold storage). **a** Surface packing density of SH-PEG5K on AuNPs as measured by ES-DMA. **b** Thickness of SH-PEG5K corona (i.e., half of the increase in particle diameter) on AuNPs as measured by ES-DMA and A4F



are noisy and do not allow the electron density profiles to be conclusively determined for the samples presented here.

In addition to surface packing density, we probed the molecular conformation of SH-PEG5K on AuNPs. SH-PEG5K, as a hydrophilic polymer, has a calculated  $\langle x^2 \rangle^{1/2}$  of 6.2 nm in water ( $a=0.6$ ). From Fig. 3b, the shell thickness (i.e., half of the increase of particle diameter) for both m-SH-PEG-AuNP and c-SH-PEG-AuNP in water (measured by A4F) was shown to be greater than  $\langle x^2 \rangle^{1/2}$ , suggesting that SH-PEG5K starts to form a brush-like corona, in contrast to the assumed random-coil conformation, on the surface of AuNPs. At the same time, the identified shell thicknesses were much less than the length of the fully extended SH-PEG5K chain (estimated at  $\approx 49$  nm by using  $a=1$  in the calculation of  $\langle x^2 \rangle^{1/2}$ ). This result suggests that SH-PEG5K may be in an intermediate state between brush-like and random-coiled conformations. The packing density was approximately 10 % of its theoretical maximum value of a short chain, self-assembled monolayer [29]. Note that the thickness of SH-PEG corona was measured by subtracting the peak size of the unconjugated AuNP monomer (i.e., core size of 23.3 nm) from the value obtained for SH-PEG-AuNP. The m-SH-PEG-AuNP sample indicates a greater thickness in both dry and wet states compared with a-SH-PEG-AuNP or c-SH-PEG-AuNP, presumably because of its high surface packing density.

Figure 3b shows a comparison between the results obtained using ES-DMA and A4F. We found the thickness of the SH-PEG corona is larger in the wet state (measured by A4F) than in the dry state (measured by ES-DMA). This is consistent with SH-PEG5K being a hydrophilic polymer that the calculated  $\langle x^2 \rangle^{1/2}$  for SH-PEG5K is 3.7 nm under dry conditions and 6.2 nm in water, respectively (i.e., theoretical values by assuming random walk coils) [29, 30]. Because a larger  $\langle x^2 \rangle^{1/2}$  in the wet state is accompanied by surface-bound water

associated with SH-PEG5K, a larger shell thickness was observed by A4F than by ES-DMA.

### Particle concentration and long-term colloidal stability

ES-DMA has proven to be an effective and quantitative approach to determine colloidal stability of AuNPs by monitoring the number-based particle size distributions of AuNPs over an extended reaction time [23]. Figure 4a shows the particle size distributions of the unconjugated AuNP and a-SH-PEG-AuNP samples after a 50-month cold storage period. We found that the unconjugated AuNPs were severely aggregated in comparison with the DMA results acquired prior to cold storage (Fig. 2a). At  $t \approx 50$  months, the distinct peaks representing monomers and dimers for unconjugated AuNPs observed at  $t=0$  month disappeared with the formation of large clusters identified via SEM imaging (Fig. 4b-1). The a-SH-PEG-AuNP sample also showed a significant degree of aggregation (Fig. 4a and b-2), but we identified both monomers ( $\approx 29$  nm) and dimers (37 nm) of detectable levels in the sample. The m-SH-PEG-AuNP and c-SH-PEG-AuNP samples were found to be very stable after this 50-month storage time (Fig. 5a), where the particle size distributions were almost unchanged with a slight change in peak  $d_{p,m}$ , suggesting that the SH-PEG5K corona provides a significant improvement to the colloidal stability of AuNPs, but is highly dependent on the functional end group. This is also echoed by the USAXS results, where the m-SH-PEG-AuNP and c-SH-PEG-AuNP data are well described by a single population of primary particles, but a population of secondary particles (aggregates) is required to obtain a reasonable fit to the a-SH-PEG-AuNP data. We surmise that the contributing factors to the observed difference in the long-term colloidal stability include [31, 32]: (1) steric repulsion by the polymer chains

**Fig. 4** Comparison of the colloidal state for unconjugated AuNPs and a-SH-PEG-AuNPs, before ( $t=0$ ) and after ( $t=50$  months) cold storage. **a** Particle diameter distribution of AuNPs after  $\approx 50$  months as measured by ES-DMA.  $Q_{sh}=30$  L  $\text{min}^{-1}$  for the  $t=0$  samples and  $Q_{sh}=10$  L  $\text{min}^{-1}$  for the  $t=50$  months samples. Sample concentrations were different for the two samples. **b** Representative SEM images after ( $t=50$  months) cold storage. 1: unconjugated AuNP; 2: a-SH-PEG-AuNP

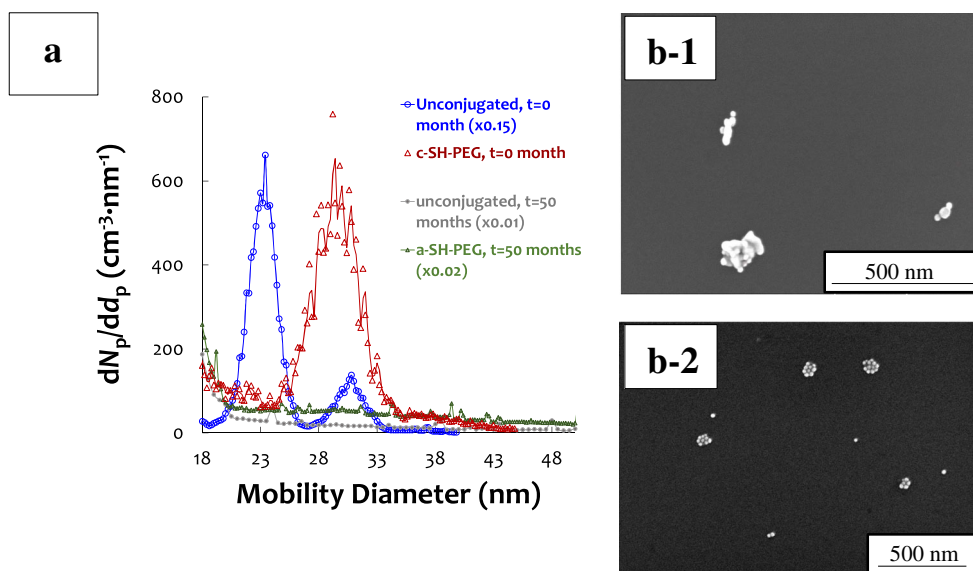
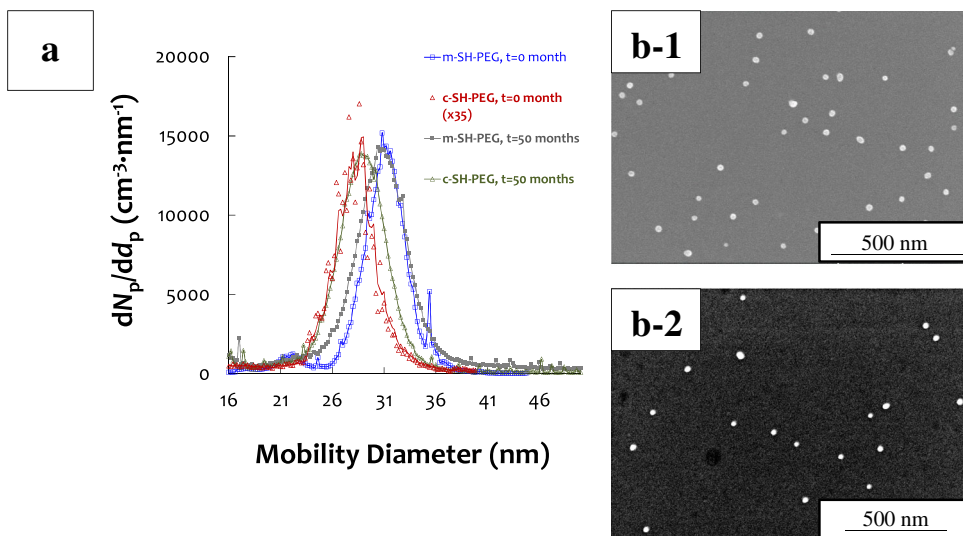


**Fig. 5** Colloidal stability of m-SH-PEG-AuNPs and c-SH-PEG-AuNPs before ( $t=0$ ) and after ( $t=50$  months) long term cold storage. **a** Particle size distribution of AuNPs at  $t=0$  and  $t=50$  months as measured by ES-DMA.  $Q_{sh}=30\text{ L min}^{-1}$  for the  $t=0$  and  $Q_{sh}=10\text{ L min}^{-1}$  for  $t=50$  months. **b** Representative SEM images after ( $t=50$  months) cold storage. 1: m-SH-PEG-AuNP; 2: c-SH-PEG-AuNP



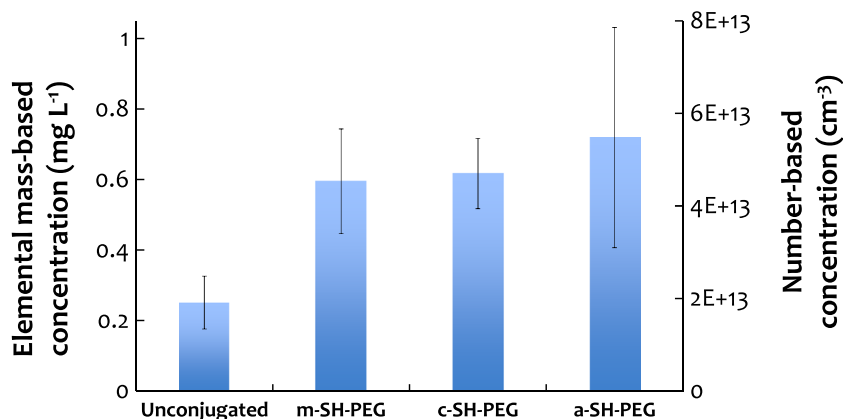
and (2) electrostatic repulsion. SEM measurements on samples at  $t\approx 50$  months, as shown in Fig. 5b-1 to b-2, further confirm the ES-DMA results. Also, we found the stability between c-SH-PEG-AuNP and a-SH-PEG-AuNP was quite different, and we attribute this difference to variations in the stock suspensions (e.g., the pH of c-SH-PEG-AuNP and a-SH-PEG-AuNP was 7.3 and 3.9, respectively). Additionally, it is important to note that significant changes in the peak size of the (SH-PEG)-conjugated AuNPs were not observed over the 50-month period (i.e., 0.2 nm for c-SH-PEG-AuNP and 0.7 nm for m-SH-PEG-AuNP), indicating that SH-PEG5K is strongly bound to Au. With >80 % of SH-PEG5K ligands remaining on the surface of AuNPs, steric repulsion between provides colloidal stability during long term cold storage.

Both number-based and mass-based concentrations of AuNPs are important to their therapeutic performance and cytotoxicity. ICP-MS was employed to study the elemental mass-based concentration of AuNPs,  $C_{m,AuNP}$ . Previous studies have shown that ICP-MS is effective in providing quantitative information on

AuNPs [21, 33–35]. As shown in Fig. 6, the  $C_{m,AuNP}$  values measured by ICP-MS following cold storage are  $2506\pm 750\text{ mg L}^{-1}$ ,  $5948\pm 1488\text{ mg L}^{-1}$ ,  $6164\pm 995\text{ mg L}^{-1}$ , and  $7187\pm 3124\text{ mg L}^{-1}$ , for unconjugated AuNPs, m-SH-PEG-AuNPs, c-SH-PEG-AuNPs, and a-SH-PEG-AuNPs, respectively (uncertainty intervals are one standard deviation for two or more replicate measurements). Using the volumetric density of AuNPs derived from a previous study ( $\rho_{AuNP}=19.2\text{ g cm}^{-3}$ ) [33] and the average primary diameter measured by TEM (21.5 nm in Fig. 1), the number-based concentrations of primary AuNPs in solution  $C_{n,AuNP}$  are estimated to be  $(2.3\pm 0.8)\times 10^{13}\text{ cm}^{-3}$ ,  $(6.0\pm 1.5)\times 10^{13}\text{ cm}^{-3}$ ,  $(6.2\pm 1.0)\times 10^{13}\text{ cm}^{-3}$ , and  $(7.2\pm 3.1)\times 10^{13}\text{ cm}^{-3}$  for unconjugated AuNPs, m-SH-PEG-AuNPs, c-SH-PEG-AuNPs, and a-SH-PEG-AuNPs, respectively (also shown in Fig. 6). These observations show that we were able to resolve the concentration of AuNPs even in a highly aggregated state; however, the inhomogeneity in sampling could contribute to measurement uncertainty.

By using a polystyrene latex (PSL) colloidal suspension with a known size and concentration as reference, the particle

**Fig. 6** Elemental mass-based concentrations and number-based concentrations of primary particles of AuNP samples measured by ICP-MS after cold storage for  $\approx 50$  months



concentrations in solution ( $N_{p,l}$ ) of m-SH-PEG-AuNP and c-SH-PEG-AuNP can be calculated from ES-DMA measurements using Eq. 2 [21, 33].

$$N_{p,l} = N_{p,g} \times \frac{N_{p,l,PS}}{N_{p,g,PS}} \quad (2)$$

Here  $N_{p,g}$  and  $N_{p,g,PS}$  are the number-based concentrations of AuNPs and PSL in the gas phase, respectively, which were calculated by integrating the peak area of the particle size distribution. From the data in Fig. 4a,  $N_{p,l}$  was found to be  $7.6 \pm 0.1 \times 10^{13} \text{ cm}^{-3}$  and  $9.3 \pm 1.0 \times 10^{13} \text{ cm}^{-3}$  for m-SH-PEG-AuNP and c-SH-PEG-AuNP, respectively. The mass-based concentrations were then calculated as  $7570 \pm 129 \text{ mg L}^{-1}$  and  $9257 \pm 1018 \text{ mg L}^{-1}$  for m-SH-PEG-AuNP and c-SH-PEG-AuNP, respectively, by assuming a particle diameter of 21.5 nm. These findings show that for both samples the measured concentration by ES-DMA is  $\approx 33\%$  higher than that derived from ICP-MS. We speculate this discrepancy is due to mass loss during sample digestion/processing for ICP-MS and/or a higher transport efficiency of AuNPs through the silica capillary for PEGylated surfaces. Experiments (not shown) have suggested that the digestion process can contribute to loss of mass for AuNPs, but a systematic study would be required to validate this effect. Optimization of the digestion process to avoid mass loss is also a viable option in this case. It should be further noted that ES-DMA is only useful to measure the concentration of AuNPs with good colloidal stability (e.g., m-SH-PEG-AuNPs and c-SH-PEG-AuNPs). Thus, we were unable to provide an accurate evaluation of concentration by ES-DMA for a-SH-PEG-AuNPs and unconjugated AuNPs after cold storage for  $\approx 50$  months, due to the substantial aggregation present in the system.

## Conclusions

In summary, a comprehensive orthogonal characterization strategy to analyze functionalized AuNPs was presented using physical/classification (ES-DMA, A4F), microscopic (TEM, SEM, AFM), and spectrometric (ICP-MS, SAXS) measurement techniques. Quantitative analysis of particle size, size distribution, particle concentration, molecular conjugation, and colloidal stability are shown to be effective through an orthogonal comparison of results. Primary size and morphology of the particles can be effectively characterized by electron microscopy or AFM imaging, but these methods cannot provide reliable information on the state of aggregation due to the limited statistical relevance and the prevalence of sample preparation artifacts. In contrast, ES-DMA, USAXS, and A4F can be used to measure the primary and secondary size and possibly to track changes in colloidal stability in a quantitative manner, but are

limited with respect to determining particle morphology. Number and mass concentration of AuNPs can be obtained by ICP-MS and ES-DMA, where ICP-MS exhibits better resolution and less restriction on the sample conditions, but ES-DMA provides single particle resolution at concentrations relevant for biomedical use. The volume size distribution of AuNPs can be obtained by small angle scattering, e.g., USAXS, which is also particularly sensitive to the presence of aggregates. Although not addressed in this work, the emerging method of single particle ICP-MS can provide single particle mass-based size and particle concentration without the need for pre-digestion of the sample; however, measurements must be conducted at very low concentrations (i.e.,  $\text{ng L}^{-1}$ ) to avoid coincident detection. We are currently exploring this approach and have published initial studies elsewhere [35]. An estimate of the number of surface-bound ligands (important for both its therapeutic and stability implications) was obtained via analysis of ES-DMA and USAXS data, with order of magnitude agreement between the two orthogonal approaches. Combining the information of the thicknesses of surface corona measured by A4F (in solution) and ES-DMA (in dry state), we can evaluate the conformation of SH-PEG on AuNPs. Finally, the multi-technique approach clearly shows that colloidal stability of AuNPs can be substantially improved for long term storage and use, by PEG-conjugation via thiol-Au bonding, which results in a high packing density and brush-like PEG corona. Importantly, up to 20% ligand loss (possibly via oxidation of the thiol group) of the SH-PEG does not appear to adversely impact colloidal stability over long periods of time, though it could affect other properties beyond the scope of this study. Our approach is broadly applicable to obtain the key material characteristics of AuNPs as described above, and can be used to help resolve critical issues related to uncertainties in material properties prior to clinical or pre-clinical evaluations.

**Acknowledgments** The authors thank Katherine Tyner at the U.S. Food and Drug Administration, Center for Drug Evaluation and Research, for providing test samples used in this study and for helpful comments. The authors also thank Hsiao-Fang Wang and Rong-Ming Ho at NTHU for assistance in TEM. DHT and YFL thank the Ministry of Science and Technology of the Republic of China (Taiwan), for financial support of this research under Contract no. Grant NSC102-2218-E-007-015-MY2.

Use of the Advanced Photon Source, an Office of Science User Facility operated for the U.S. Department of Energy (DOE) Office of Science by Argonne National Laboratory, was supported by the U.S. DOE under Contract No. DE-AC02-06CH11357. ChemMatCARS Sector 15 is principally supported by the Divisions of Chemistry (CHE) and Materials Research (DMR), National Science Foundation, under grant number NSF/CHE-1346572.

**Conflict of interest** The authors declare no conflict of interest.

## References

1. Jokerst JV, Lobovkina T, Zare RN, Gambhir SS (2011) *Nanomedicine-UK* 6:715–728
2. Giljohann DA, Seferos DS, Daniel WL, Massich MD, Patel PC, Mirkin CA (2010) *Angew Chem Int Ed* 49:3280–3294
3. Yeh YC, Creran B, Rotello VM (2012) *Nanoscale* 4:1871–1880
4. Ng VWK, Berti R, Lesage F, Kakkar A (2013) *J Mater Chem B* 1:9–25
5. Webb JA, Bardhan R (2014) *Nanoscale* 6:2502–2530
6. Lee SM, Tsai DH, Hackley VA, Brechbiel MW, Cook RF (2013) *Nanoscale* 5:5252–5256
7. Eustis S, El-Sayed MA (2006) *Chem Soc Rev* 35:209–217
8. Daniel MC, Astruc D (2004) *Chem Rev* 104:293–346
9. Nelson BC, Petersen EJ, Marquis BJ, Atha DH, Elliott JT, Cleveland D, Watson SS, Tseng IH, Dillon A, Theodore M, Jackman J (2013) *Nanotoxicology* 7:21–29
10. Paciotti GF, Kingston DGI, Tamarkin L (2006) *Drug Develop Res* 67:47–54
11. Tsai DH, Elzey S, DelRio FW, Keene AM, Tyner KM, Clogston JD, MacCuspie RI, Guha S, Zachariah MR, Hackley VA (2012) *Nanoscale* 4:3208–3217
12. Cho TJ, MacCuspie RI, Gigault J, Gorham JM, Elliott JT, Hackley VA (2014) *Langmuir* 30:3883–3893
13. Keene AM, Allaway RJ, Sadrieh N, Tyner KM (2011) *Nanotoxicology* 5:469–478
14. Keene AM, Peters D, Rouse R, Stewart S, Rosen ET, Tyner KM (2012) *Nanomedicine-UK* 7:618
15. Wei A, Mehtala JG, Patri AK (2012) *J Control Release* 164:236–246
16. Adisheshaiah PP, Hall JB, McNeil SE (2010) *WIREs Nanomed Nanobiotechnol* 2:99–112
17. Fubini B, Fenoglio I, Tomatis M, Turci F (2011) *Nanomedicine-UK* 6:899–920
18. Wang J, Byrne JD, Napier ME, DeSimone JM (2011) *Small* 7: 1919–1931
19. Parrott MC, DeSimone JM (2012) *Nat Chem* 4:13–14
20. Perry JL, Reuter KG, Kai MP, Herlihy KP, Jones SW, Luft JC, Napier M, Bear JE, DeSimone JM (2012) *Nano Lett* 12:5304–5310
21. Tsai DH, Cho TJ, Elzey SR, Gigault JC, Hackley VA (2013) *Nanoscale* 5:5390–5395
22. The identification of any commercial product or trade name does not imply endorsement or recommendation by the National Institute of Standards and Technology
23. Tsai DH, Cho TJ, DelRio FW, Taurozzi J, Zachariah MR, Hackley VA (2011) *J Am Chem Soc* 133:8884–8887
24. Tsai DH, DelRio FW, Keene AM, Tyner KM, MacCuspie RI, Cho TJ, Zachariah MR, Hackley VA (2011) *Langmuir* 27:2464–2477
25. Ilavsky J, Jemian PR, Allen AJ, Zhang F, Levine LE, Long GG (2009) *J Appl Crystallogr* 42:469–479
26. Ilavsky J, Jemian PR (2009) *J Appl Crystallogr* 42:347–353
27. Crist RM, Grossman JH, Patri AK, Stern ST, Dobrovolskaia MA, Adisheshaiah PP, Clogston JD, McNeil SE (2013) *Integr Biol-UK* 5: 66–73
28. Reports of Investigation: SRM8011, SRM8012, SRM8013, National Institute of Standards and Technology, United States of America
29. Tsai DH, DelRio FW, MacCuspie RI, Cho TJ, Zachariah MR, Hackley VA (2010) *Langmuir* 26:10325–10333
30. Tsai DH, Davila-Morris M, DelRio FW, Guha S, Zachariah MR, Hackley VA (2011) *Langmuir* 27:9302–9313
31. Vericat C, Vela ME, Benitez G, Carro P, Salvarezza RC (2010) *Chem Soc Rev* 39:1805–1834
32. Maus L, Spatz JP, Fiammengo R (2009) *Langmuir* 25:7910–7917
33. Elzey S, Tsai DH, Yu LL, Winchester MR, Kelley ME, Hackley VA (2013) *Anal Bioanal Chem* 405:2279–2288
34. Hinterwirth H, Kappel S, Waitz T, Prohaska T, Lindner W, Lammerhofer M (2013) *ACS Nano* 7:1129–1136
35. Liu JY, Murphy KE, MacCuspie RI, Winchester MR (2014) *Anal Chem* 86:3405–3414



**De-Hao Tsai** is an Assistant Professor at the Department of Chemical Engineering, National Tsing Hua University, Taiwan. His research interests include nanomaterial characterization, surface chemistry of nanomaterials for the optimization of formulation chemistry, and the fabrication of functional nanoparticles for biomedical and energy applications.



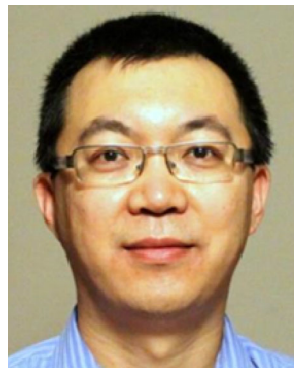
**Yi-Fu Lu** is a graduate research assistant at the Department of Chemical Engineering, National Tsing Hua University, Taiwan. His main research work is to develop in-situ and ex-situ analytical approaches to characterize the activity of nano-catalysts.



**Frank W. DelRio** is a research scientist in the Applied Chemicals and Materials Division at the National Institute of Standards and Technology (NIST) in Boulder, CO. His research interests include measurements and standards related to the elastic, plastic, fracture, interfacial, and charge transport properties of thin films and small-scale structures.



**Tae Joon Cho** is currently a research associate at Materials Measurement Science Division, National Institute of Standards and Technology and he has been working for many years on development of stable, functional engineered nanomaterials and their utilization for biological application; (synthesis, characterization, stability study). His research background also includes synthesis and characterization of dendrimers, self-assembled supramolecules, and biomimic polymers.



**Fan Zhang** is a physicist at the Material Measurement Laboratory, National Institute of Standards and Technology in Gaithersburg, United States. His research focuses on the development and application of small angle X-ray scattering and its related techniques to probe the static microstructure and dynamics of a wide range of materials, particularly those of colloids, polymers, and polymer composites.



**Suvajyoti Guha** is an expert in bionanoparticle characterization and is currently associated with US Food and Drug Administration as a post-doctoral fellow where he conducts research on medical devices. Before his current stint, he was a guest researcher at NIST, Gaithersburg where he looked at a variety of problems pertaining to viral degradation, protein aggregation, protein adsorption and drug-protein conjugates.



**Andrew Allen** is a physicist in the Materials Measurement Science Division of the Material Measurement Laboratory at the U.S. Department of Commerce's National Institute of Standards and Technology (NIST). His main research interests focus on advanced materials in support of U.S. Government programs and industry, together with the development and application of novel neutron and X-ray scattering methods needed for these studies. Currently, he is also one of the three main editors of the *Journal of Applied Crystallography*.



**Michael R. Zachariah** is Patrick and Marguerite Sung Distinguished Professor of Chemical Engineering and Chemistry. He has expertise in aerosol generated materials and has published extensively on metrology of nanoparticles in both the liquid and gas phases.



**Vincent A. Hackley** is leader of the project on *Nanoparticle Metrology for Health and the Environment* at the National Institute of Standards and Technology, a non-regulatory agency within the U.S. Department of Commerce. This multidisciplinary research effort focuses on development of methods for separation, characterization and quantification of engineered nanoparticles, their coatings, and their transformation products, with a particular emphasis on hyphenated techniques. He is also involved in efforts to develop nanoscale reference materials, which are utilized worldwide.